

1     **The sensitivity of landfast sea ice to atmospheric forcing in**  
2     **single-column model simulations: a case study at Zhongshan**  
3                     **Station, Antarctica**

4                     Fengguan Gu<sup>1</sup>, Qinghua Yang<sup>1</sup>, Frank Kauker<sup>2,3</sup>, Changwei Liu<sup>1</sup>, Guanghua Hao<sup>4</sup>,  
5                     Chao-yuan Yang<sup>1</sup>, Jiping Liu<sup>5</sup>, Petra Heil<sup>6</sup>, Xuewei Li<sup>1</sup>, Bo Han<sup>1\*</sup>

6     1 School of Atmospheric Sciences, Sun Yat-sen University, and Southern Marine Science and Engineering  
7     Guangdong Laboratory (Zhuhai), Zhuhai 519082, China

8     2 Alfred Wegener Institute, Helmholtz Centre for Polar and Marine Research, Am Handelshafen 12, 27570  
9     Bremerhaven, Germany

10    3 Ocean Atmosphere Systems, Tevesstseg 4, 20249 Hamburg, Germany

11    4 Key Laboratory of Marine Hazards Forecasting, National Marine Environmental Forecasting Center, Ministry of  
12    Natural Resources, Beijing 100081, China

13    5 Department of Atmospheric and Environmental Sciences, State University of New York at Albany, Albany, NY,  
14    USA

15    6 Australian Antarctic Division and Australian Antarctic Program Partnership, Private Bag 80, Hobart, Tas 7001,  
16    Australia

17    Correspondence to: Bo Han (hanb5@mail.sysu.edu.cn)

18

19     **Abstract**

20         Single-column sea ice models are used to focus on the thermodynamic evolution of the ice.  
21     Generally, these models are forced by atmospheric reanalysis in the absence of atmospheric *in situ*  
22     observations. Here we assess the sea ice thickness (SIT) simulated by a single-column model  
23     (ICEPACK) with *in situ* observations obtained off Zhongshan Station for the austral winter of 2016.  
24     In the reanalysis, the surface air temperature is about 1 °C lower, the total precipitation is about 2  
25     mm day<sup>-1</sup> larger, and the surface wind speed is about 2 m s<sup>-1</sup> higher compared to the *in situ*  
26     observations, respectively. We designed sensitivity experiments to evaluate the simulation bias in  
27     sea ice thickness due to the uncertainty in the individual atmospheric forcing variables. Our results  
28     show that the unrealistic precipitation in the reanalysis leads to a bias of 14.5 cm in sea ice thickness  
29     and 17.3 cm in snow depth. In addition, our data show that increasing snow depth works to gradually

30 inhibit the growth of sea ice associated with thermal blanketing by the snow due to changing the  
31 vertical heat flux. Conversely, given suitable conditions, the sea ice thickness may grow suddenly  
32 when the snow load gives rise to flooding and leads to snow-ice formation. However, there are still  
33 uncertainties related to the model results, because superimposed ice and snowdrift are not  
34 implemented in the used version of the ice model and because snow-ice formation might be  
35 overestimated at locations with landfast sea ice.

36

## 37 **1 Introduction**

38 Sea ice plays an essential role in the global climate system by reflecting solar radiation and  
39 regulating the heat, moisture, and gas exchanges between the ocean and the atmosphere. In contrast  
40 to the rapid decline of sea ice extent and volume in the Arctic (Stroeve et al., 2012; Lindsay and  
41 Schweiger, 2015), satellite observations show a slight increase in the yearly-mean area of Antarctic  
42 sea ice since the late 1970s (Parkinson and Cavalieri, 2012) followed by a rapid decline from 2014  
43 (Parkinson, 2019) and a renewed increase in most recent years (Chemke and Polvani, 2020).  
44 Although the sudden decline of Antarctic sea ice is yet to be attributed (Parkinson, 2019), the spatial  
45 pattern of Antarctic sea ice changes is suggested to be primarily caused by changes in the  
46 atmospheric forcing. For example, the rapid ice retreat in the Weddell Sea from 2015 to 2017 has  
47 been associated with the intensification of northerly wind (Turner et al., 2017), while the phase of  
48 the southern annular mode (SAM) significantly modulates the sea ice in the Ross Sea and elsewhere,  
49 especially in November 2016 (Stuecker et al., 2017; Schlosser et al., 2018; Wang et al., 2019a).

50 Landfast sea ice, the immobile fraction of the sea ice, is mainly located near coastal regions of  
51 Antarctica, and its change is assumed to be indicative of the evolution of total Antarctic sea ice (Heil  
52 et al., 1996; Heil, 2006; Lei et al., 2010; Yang et al., 2016a). Unlike drifting sea ice, the change in  
53 landfast sea ice is dominated by thermodynamic processes, which single-column sea-ice models can  
54 well capture (Heil et al., 1996; Lei et al., 2010; Yang et al., 2016b; Zhao et al., 2017; Liu et al.,  
55 2022). Furthermore, a single-column sea ice model is a useful tool to evaluate the impacts of  
56 different atmospheric forcings on the sea ice evolution because of the relatively simple structure of  
57 the physical processes (Cheng et al., 2013; Wang et al., 2019b; Merkouriadi et al., 2020). In this  
58 study, a state-of-the-art single-column sea ice model, ICEPACK, is chosen to investigate the  
59 sensitivity of landfast sea ice to atmospheric forcing for the region off Zhongshan Station in Prydz

60 Bay, East Antarctica (Figure 1).

61 Due to the lack of *in situ* observation, the majority of sea ice studies, especially for the Antarctic,  
62 rely on numerical models. Realistic atmospheric forcing is critical for reliable model simulations.  
63 Although being criticized for significant deviations from *in situ* observations (Bromwich et al., 2007;  
64 Vancoppenolle et al., 2011; Wang et al., 2016; Barthélemy et al., 2018), atmospheric reanalysis data  
65 are assumed to offer reasonable atmospheric forcing for large-scale sea ice models for the Antarctic  
66 (Zhang, 2007; Massonnet et al., 2011; Zhang, 2014; Barthélemy et al., 2018). Previous studies  
67 reported a large spread between four global atmospheric reanalysis products and *in situ* observations  
68 in the Amundsen Sea Embayment (Jones et al., 2016). Moreover, studies showed that directly using  
69 atmospheric reanalysis as forcing for models causes significant biases in the Arctic sea ice  
70 simulations (Lindsay et al., 2014; Wang et al., 2019b). Similar results, accentuated by the sparseness  
71 of atmospheric observations entering the reanalysis, can be foreseen for Antarctica. Therefore, the  
72 atmospheric forcing needs to be evaluated carefully before simulating Antarctic sea ice. To our  
73 knowledge, few studies have given a quantitative evaluation of the effect of different atmospheric  
74 forces on sea ice simulations in Antarctica.

75 The coastal landfast sea ice in Prydz Bay is generally first-year ice. It usually fractures and is  
76 exported or melts out completely between December and the following February, and refreeze  
77 occurs from late February onwards (Lei et al., 2010). This seasonal cycle is representative of  
78 Antarctic landfast sea ice. This study aims to evaluate the contributions of the various atmospheric  
79 forcing variables on landfast sea ice growth. The snow cover exerts influence on the evolution of  
80 the vertical sea ice-snow column via a number of mechanisms, including the formation of snow-ice  
81 added by flooding (Leppäranta, 1983), superimposed ice (Kawamura et al., 1997), and insulating  
82 impact (Massom et al., 2001). Understanding the snow depth is a primary concern here.

83 Two sets of atmospheric forcing have been chosen. The first is spatially interpolated ERA5 onto  
84 the location of the observation site, and the second is using *in situ* atmospheric observations. It is  
85 well-known that the simulation biases of numerical models are introduced through many  
86 shortcomings, including unrealistic surface boundary conditions (here: atmospheric forcing),  
87 imperfect physical process formulations, computational errors. Understanding the uncertainty in sea  
88 ice simulations as well as the sea ice response pattern to atmospheric forcing due to imperfect  
89 surface boundaries is a prerequisite for successful simulations and needs to be assessed first.

90 This study is arranged as follows: Section 2 introduces the *in situ* observations, the numerical  
91 model, and the reanalysis. The main results are given in section 3, focusing on different kinds of  
92 atmospheric forcing on sea ice and snow. Shortcomings, discussions and conclusions follow in  
93 sections 4, 5 and 6.

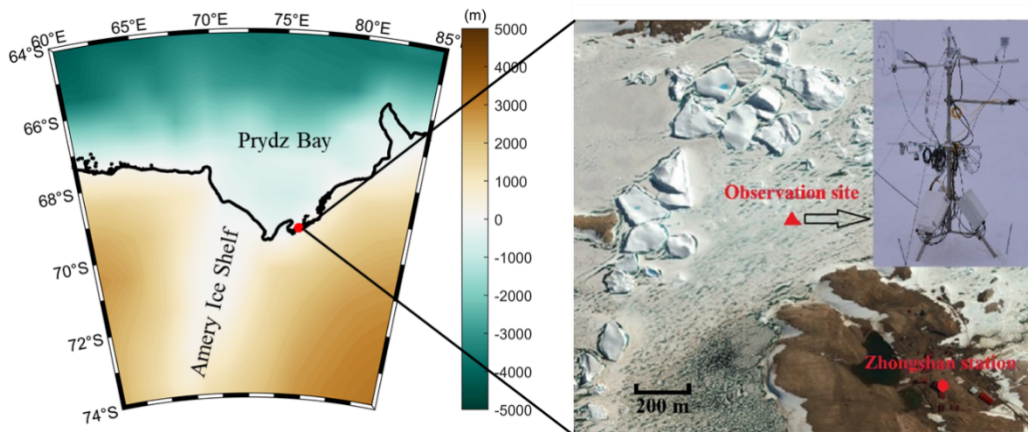
94

## 95 2 Materials and methods

### 96 2.1 Meteorological observations

97 The site of sea ice observation locates in the coastal area off Zhongshan Station  
98 [(69°22'S,76°22'E); Figure 1], East Antarctica. The meteorological data were collected at a year-  
99 round manned weather observatory run at Zhongshan Station in 2016, which is 1 km inland from  
100 the sea ice observation site and 15 m above sea level. Snowfall is measured every 12 hours at the  
101 Russian Progress II station (located ~1 km to the southeast of Zhongshan Station). The short- and  
102 long-wave radiation fluxes were measured every minute with a net radiometer mounted 1.5 m above  
103 the surface on a tripod (Yang et al., 2016a). Other meteorological variables are available as hourly  
104 data, including 2 m air temperature ( $T_{2m}$ ), surface pressure ( $P_a$ ), specific humidity (calculated from  
105 dew-point temperature and  $P_a$ ), potential temperature (calculated from  $T_{2m}$  and  $P_a$ ), air density  
106 (calculated by  $T_{2m}$  and  $P_a$ ) and 10 m wind speed ( $U_{10}$ ) (Hao et al., 2019; Hao et al., 2020; Liu et al.,  
107 2020).

108



109

110 Figure 1 Location of landfast sea ice surface measurements near Zhongshan Station. The solid  
111 triangle denotes the observation site, the solid circle marks Zhongshan Station. The color on the left  
112 represents the terrain.

113

114

## 115 **2.2 Sea ice thickness measurement**

116 A thermistor-chain unit developed by Taiyuan University of Technology (TY) was used to  
117 measure sea ice thickness in austral winter 2016. This unit is composed of two parts: the control unit  
118 and the thermistor chain. The controller initiates data acquisitions and records and stores the  
119 temperature measurements. The thermistor chain is 3 m long with 250 equidistant thermistors. Their  
120 sensitivity is 0.063 °C, and the measurement accuracy is  $\pm 0.1$  °C. The thermistor chain  
121 simultaneously records the vertical temperature profile across the near-surface atmosphere, snow  
122 cover, sea ice, and surface seawater. The measurement frequency is hourly. Details about the  
123 instruments can be found in Hao et al. (2019).

124 Snow thickness close to the thermistor unit is measured weekly using a ruler with an accuracy  
125 of  $\pm 0.2$  cm. Sea ice thickness is measured with a ruler through a drill hole (5 cm diameter) weekly.  
126 The measurement accuracy is  $\pm 0.5$  cm. The average thickness obtained from three close-by sites is  
127 retained. Sea-surface temperature and sea-surface salinity are measured in the drill holes weekly  
128 using a Cond 3210 set 1 (Hao et al., 2019).

129

## 130 **2.3 Atmospheric reanalysis data**

131 The European Centre for Medium-range Weather Forecasts (ECMWF) released ERA5, the new  
132 reanalysis product in 2017, updated in near real-time (Hersbach and Dee, 2016; Hersbach et al.,  
133 2020). The complete ERA5 dataset, extending back to 1950, has been available to the end of 2019  
134 during this study. Compared with the popular ERA-Interim reanalysis, there are several significant  
135 improvements in ERA5, including much higher resolutions (both spatially and temporally). ERA5  
136 has global coverage with a horizontal resolution of 31 km by 31 km at the equator and 10 km by 31  
137 km at the latitude of Zhongshan Station. The ERA5 resolves the vertical atmosphere profile using  
138 137 vertical pressure levels from the surface up to a geopotential height of 0.01 hPa. ERA5 provides  
139 hourly analysis and forecast fields and applies a four-dimensional variational data assimilation  
140 system (4D-var). ERA5 includes various reprocessed quality-controlled data sets, for example, the  
141 reprocessed version of the Ocean and Sea Ice Satellite Application Facilities (OSI SAF) sea ice  
142 concentration (Hersbach and Dee, 2016; Hersbach et al., 2020).

143 For comparison and evaluation against the observation in this study, gridded data from ERA5  
 144 has been bilinearly interpolated to the observation site (detailed in 2.1). Directly using atmospheric  
 145 forcing from coarse grid cells to interpolate to the observation site, although widely accepted in the  
 146 previous studies (e.g., Urraca et al., 2018; Wang et al., 2019b), may cause errors. We have checked  
 147 the performance of ERA5 and found that the spatial difference of surface atmospheric variables  
 148 around the observation site is relatively small, indicating the choice of interpolation techniques will  
 149 not affect the conclusion of this study.

150

## 151 2.4 ICEPACK

152 ICEPACK is a column-physics component of the Los Alamos Sea Ice Model (CICE) V6 and is  
 153 maintained by the CICE Consortium. ICEPACK incorporates column-based physical processes that  
 154 affect the area and thickness of sea ice. It includes several options for simulating sea ice  
 155 thermodynamics, mechanical redistribution (ridging), and associated area and thickness changes. In  
 156 addition, the model supports several tracers, including ice thickness, enthalpy, ice age, first-year ice  
 157 area, deformed ice area and volume, melt ponds, and biogeochemistry (Hunke et al., 2019).  
 158 ICEPACK Version 1.1.1 was used in this study, and detailed options of physical  
 159 parameterizations and model settings for the ICEPACK are summarized in Table 1. We employ  
 160 ICEPACK to distribute the initial ice thickness to each ice thickness category using a distribution  
 161 function:

$$162 \quad p_i = \frac{\max(2 \times h \times H_i - H_i^2, 0)}{\sum_i \max(2 \times h \times H_i - H_i^2, 0)}, i = 1 \dots N, (1)$$

163 Where  $h$  is the initial ice thickness,  $H_i$  is the prescribed ice thickness category (0–0.6, 0.6–1.4, 1.4–  
 164 2.4, 2.4–3.6, and above 3.6 m~; same as for Arctic simulations),  $N$  is the number of ice thickness  
 165 categories.

166 Table 1 Detailed options of physical parameterizations and model settings for the ICEPACK.

ICEPACK	Value
time step	3600 s
Number of layers in the ice	7
Number of layers in the snow	1
Ice thickness categories	5 (Bitz et al., 2001)
Initial ice thickness	99.5 cm (observed)
Initial snow depth	11.5 cm (observed)
Albedo scheme	CCSM3 (Collins et al., 2006)

Ice thermodynamic	Mushy-layer (Turner et al., 2013)
Shortwave radiation	Delta-Eddington (Briegleb and Light, 2007)
Snowdrift	Not implemented in ICEPACK 1.1.1
Melt ponds (superimposed ice)	Not used in this study
Ocean heat transfer coefficient	0.006 (Maykut and McPhee, 1995)
SST restoring time scale (days)	0 (use observed SST as oceanic forcing)
Ocean friction velocity minimum (m/s)	0.0005 (Tsamados et al., 2013)

---

167 The atmospheric forcing for the ICEPACK model consists of observations of downward short-  
168 and long-wave radiation, 2 m air temperature, specific humidity, total precipitation, potential  
169 temperature, 2 m air density, and 10 m wind speed. The oceanic forcing includes sea surface  
170 temperature, sea surface salinity, and oceanic mixed layer depth. The period concerned in this study  
171 is from April 22, when observed sea ice generally starts to grow, to November 22, 2016. Since there  
172 are no observations of the ocean’s mixed-layer depth, we set it to 10 m based on a previously  
173 published study (Zhao et al., 2019).

174

### 175 **3 Results**

#### 176 **3.1 Surface atmospheric conditions near the observation site**

177 First, we compare the eight atmospheric variables used to force ICEPACK (surface downward  
178 shortwave radiation ( $R_{sd}$ ), surface downward long-wave radiation ( $R_{ld}$ ), surface air temperature ( $T_a$ ),  
179 specific humidity ( $Q_a$ ), precipitation ( $P$ ), air potential temperature ( $\theta_a$ ), air density ( $\rho_a$ ), wind speed  
180 ( $U_a$ ) with the respective *in situ* observation. Table 2 lists the bias (reanalysis minus observation),  
181 bias ratio (ratio between the bias and the observation value), the mean value of the *in situ* observation  
182 (Mean\_Obs), the correlation coefficient (Corr.), and the root-mean-square deviation (RMSD)  
183 between the interpolated ERA5 data and the observation. In general, all eight variables from the two  
184 sources closely follow each other (Corr. > 0.85), except for  $P$  and  $U_a$ . In this study, the main attention  
185 is on the atmospheric variables  $T_a$ ,  $P$ , and  $U_a$  for three reasons: (1) Previous studies have shown that  
186 from all atmospheric forcing variables, uncertainties in  $T_a$ ,  $P$ , and  $U_a$  exert a significant impact on  
187 the sea ice thickness (Cheng et al., 2008). (2) Surface wind may affect the snow cover in two ways:  
188 sublimation due to surface turbulent heat flux (Fairall et al., 2003; Gascoïn et al., 2013) and the  
189 snowdrift process (Thiery et al., 2012). (3)  $P$  and  $U_a$  from the reanalysis have the largest bias ratio  
190 compared to the *in situ* observations.

191 The timing of daily variations of  $T_a$  is well represented by ERA5, especially for strong cooling

192 events (Figure 2a). However, ERA5 tends to underestimate warm events by a few degrees as well  
 193 as cold events where differences exceeding 10 °C may occur (Figure 2d). During the entire  
 194 observation period in 2016,  $T_a$  from ERA5 was 1.2 °C lower than the *in situ* observation. Also,  
 195 previous studies reported similar disagreement in  $T_a$  between observation and reanalysis in  
 196 Antarctica (Bracegirdle and Marshall, 2012; Fréville et al., 2014). The cold bias of  $T_a$  in the  
 197 reanalysis was suggested to be caused by the ice surface schemes that cannot accurately describe  
 198 the ice-atmosphere interactions of strongly stable stratified boundary layers that are frequent in  
 199 Antarctica.

200

201 Table 2 Comparison of atmospheric forcing between ERA5 reanalysis and *in situ* observations.

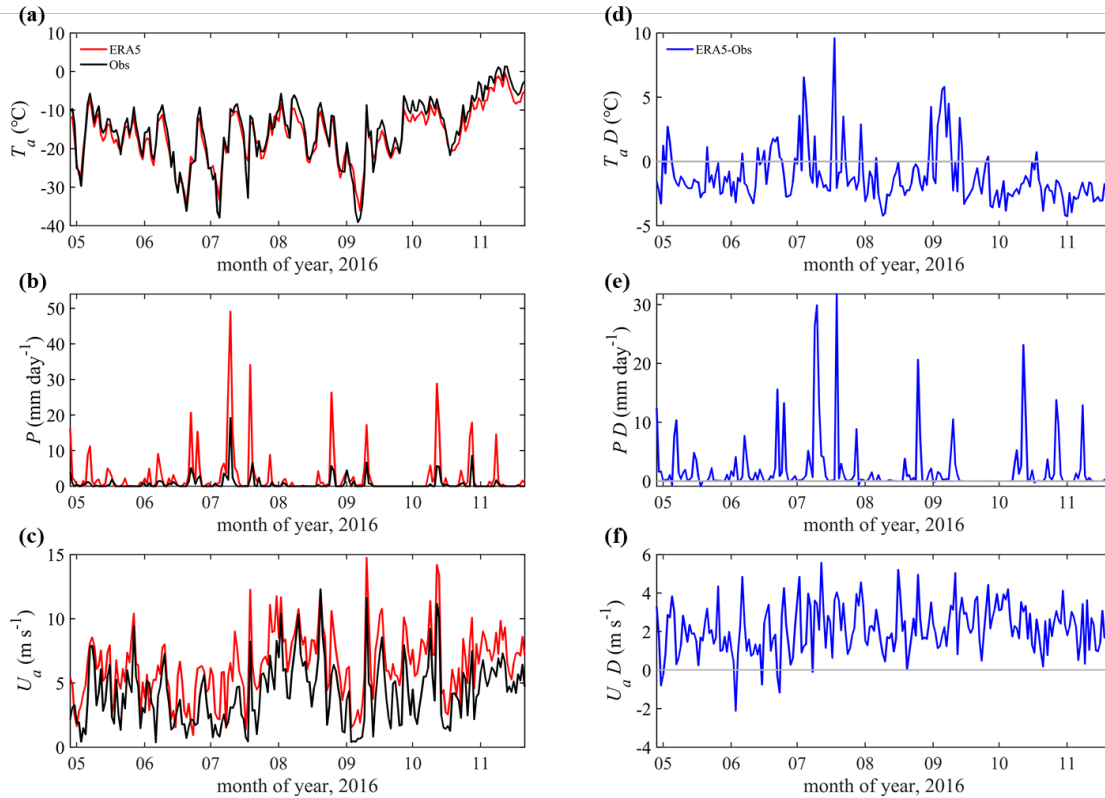
Variable	Bias	Bias ratio (%)	Mean_Obs	Corr	RMSD
$R_{sd}$ (W m <sup>-2</sup> )	6.115	9.031	67.714	0.967	40.981
$R_{ld}$ (W m <sup>-2</sup> )	-19.153	-9.672	198.023	0.869	28.753
$T_a$ (K)	-1.168	-0.453	257.809	0.967	2.820
$Q_a$ (10 <sup>-4</sup> kg kg <sup>-1</sup> )	-0.769	-9.326	8.247	0.950	1.987
$P$ (mm day <sup>-1</sup> )	2.010	303.509	0.660	0.639	0.825
$\Theta_a$ (K)	0.290	0.112	259.437	0.965	2.609
$\rho_a$ (kg m <sup>-3</sup> )	-0.021	-1.592	1.322	0.958	0.026
$U_a$ (m s <sup>-1</sup> )	2.145	50.735	4.228	0.765	2.989

202

203 The reanalyzed variable with the largest bias ratio from the observation is precipitation (Figure  
 204 2b). Hourly precipitation from ERA5 was accumulated into daily data and compared with the  
 205 nearest available daily precipitation records from the Progress II station. The maximum daily mean  
 206 precipitation can reach 19.1 mm day<sup>-1</sup> (July 11, 2016), with an average of 0.66 mm day<sup>-1</sup> from April  
 207 29 to November 22, 2016. While ERA5 captures the main precipitation events, it significantly  
 208 overestimated the magnitude of precipitation events, especially in July. In this month, the mean  
 209 precipitation rate from ERA5 is 5.83 mm day<sup>-1</sup>, while the observed is only 1.42 mm day<sup>-1</sup>. From  
 210 April to November, the accumulated precipitation from ERA5 is about 300% larger than that in the  
 211 *in situ* observations. Nevertheless, using precipitation from Progress II for Zhongshan Station may  
 212 be questioned because of the distance of about 1 km to Zhongshan Station. Moreover, the snowdrift  
 213 due to strong surface wind can affect the precipitation observation and the local accumulated snow  
 214 mass, which may further cause a significant bias in snow depth between simulation and observation.



215  
216



217

218 Figure 2 Time series of daily (a) surface air temperature, (b) precipitation rate, and (c) wind speed  
219 (10 m above the surface). The ERA5 reanalysis data are indicated as red lines. Observations are  
220 marked by black lines. (d-f) show the difference (marked by 'D') between ERA5 and the observation  
221 (ERA5-observation). The differences are marked by blue lines. The gray lines denote the zero line.  
222

223 The observed  $U_a$  varied from 0.01 m s<sup>-1</sup> to 12.3 m s<sup>-1</sup> with an average of 4.2 m s<sup>-1</sup> (Figure 2c).  
224 ERA5 well captured the daily and seasonal variation of  $U_a$ , but an overestimation of 2.1 m s<sup>-1</sup> should  
225 be noted, mainly when observed  $U_a > 5$  m s<sup>-1</sup>. One explanation for such overestimation is that the  
226 numerical model underlying ERA5 cannot represent the surface roughness and the katabatic wind  
227 in a region with complex orography (Tetzner et al., 2019; Vignon et al., 2019).  
228

228

### 229 3.2 Simulation forced by observed *in situ* atmospheric variables

230 The simulation bias of sea ice thickness and snow depth is impacted by many aspects, including  
231 unrealistic atmospheric and oceanic forcing and shortcomings in the applied numerical model. In  
232 this study, we mainly focus on the influence of imperfect atmospheric forcing.

233 The sea ice thickness (Obs) measured through a hole drilled is increasing from April 29 ( $100\pm 2$   
234 cm) to October 25 ( $172\pm 2$  cm), remaining level from there on (Figure 3a). The ice thickness deduced  
235 from the TY (Obs\_TY) thermistor-chain buoy shows a similar result: sea ice thickness increased  
236 from 106 cm on April 22 to 171 cm on November 17. In November, the sea ice thickness (Obs and  
237 Obs\_TY) is stationary, indicating a thermodynamic equilibrium between heat loss to the atmosphere  
238 and heat gain from the ocean (Yang et al., 2016a; Hao et al., 2019).

239 When forced by atmospheric *in situ* observations (Sim\_Obs), the simulated sea ice thickness  
240 agrees well with the observed thickness with a mean bias of less than 1 cm over the growing season.  
241 We attribute the excellent simulation result to the fact that the seasonal evolution of landfast is driven  
242 mainly by thermal processes, which ICEPACK captures well.

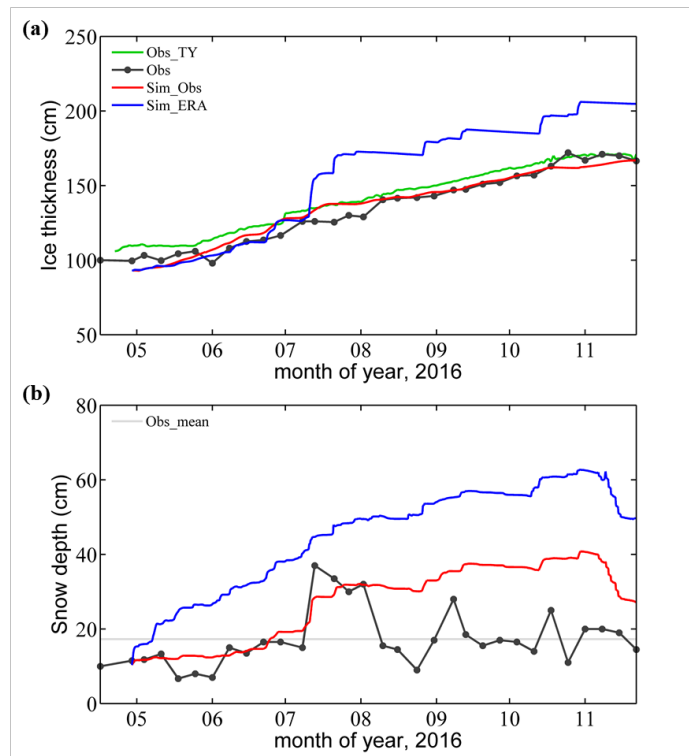
243 The average snow depth from observation is 17 cm during the ice-growth season, with low snow  
244 depth measured before July 11 (Figure 3b). After that, the snow depth increases rapidly up to about  
245 37 cm, associated with a precipitation event arising from a single synoptic system. Then it decreases  
246 below the seasonal mean (Obs\_mean), followed by two secondary maxima ( $> 25$  cm) on September  
247 8 and October 18, respectively.

248 The snow depth in Sim\_Obs tracks the observation closely before August 2 (Figure 3b). Then,  
249 the Observed snow depth decreased quickly from about 30 cm to about 10 cm, while the Sim\_Obs  
250 snow depth continued to increase gradually until the onset of surface melting in November. We  
251 attribute the Observed quick decrease of snow depth to the effect of the snowdrift because the  
252 surface wind stayed above  $5 \text{ m s}^{-1}$  for most of August (Figure 2c), giving rise to snowdrift, a process  
253 not implemented in the version of ICEPACK used here. The snowdrift might cause a significant  
254 spatial difference in accumulated snow patterns (Liston et al., 2018), which may be responsible for  
255 the large deviation in snow depth between Sim\_Obs and Observation. In addition, Sim\_Obs  
256 underestimated the snow depth on July 11. As discussed above, using nonlocal observed  
257 precipitation from Progress II should be questioned.

258 Using observed meteorological variables as atmospheric forcing in ICEPACK produced  
259 unreliable snow depth while the sea ice thickness was in reasonably good agreement. In other words,  
260 the enormous bias in snow depth seems to have little effect on the sea ice thickness in the simulation.  
261 This counter-intuitive finding is of great interest to us because it disobeys the general realization  
262 that the snow layer significantly modifies the energy exchange on top of the sea ice. Potential causes

263 for this result will be discussed later.

264



265

266 Figure 3 Time series of (a) sea ice thickness and (b) snow depth during the freezing season. Black  
267 solid lines with black points show the observations from the drill hole (Obs). Green solid lines show  
268 the ice thickness derived from the TY buoy (Obs\_TY). Red solid lines show the simulation results  
269 under *in situ* atmospheric forcing (Sim\_Obs), and blue solid lines are simulation results under ERA5  
270 forcing (Sim\_ERA). In (b), the gray solid line shows the seasonal mean snow depth observation  
271 (Obs\_mean).

272

### 273 3.3 Simulation forced by ERA5 atmospheric variables

274 When forced by ERA5 (Sim\_ERA), the simulated sea ice thickness shows significant deviations  
275 from observation (Figure 3a). The deviation is only about 1 cm before July 11, when a heavy  
276 precipitation event ( $\sim 19 \text{ mm day}^{-1}$ ) happened. After the precipitation episode, the offset in the sea  
277 ice thickness between Sim\_ERA and observation was almost constant, about 33 cm.

278 In contrast to sea ice thickness, the precipitation from ERA5 causes an overestimation in snow  
279 depth for the entire simulation period. The snow depth from Sim\_ERA is much greater than  
280 observation, even before July 11 (Figure 3b). During the heavy precipitation event (Figure 2b), the

281 observed snow depth increased from 20 cm to about 40 cm. Although the precipitation rate from  
 282 ERA5 ( $\sim 40 \text{ mm day}^{-1}$ ) is two times larger than the observation, it caused little response in the  
 283 simulated snow depth. The snow depth increase is near-linear, from about 10 cm to almost 60 cm.  
 284

### 285 3.4 Sensitivity analysis

286 To determine which atmospheric variables, including  $T_a$ ,  $P$ , and  $U_a$ , are the most crucial in the  
 287 sea ice simulation, we designed a set of sensitivity simulation experiments named SEN1. The  
 288 simulation under the forcing from the *in situ* observed atmospheric variables is the control  
 289 experiment and is named Sim\_Obs. In each experiment of SEN1, one atmospheric variable is  
 290 replaced by the corresponding variable from ERA5, while all others are identical to those of the  
 291 control experiment. In Table 3, the averaged bias between the simulation and the observation of the  
 292 outputs (ice thickness and snow depth) and the bias ratio of forcing atmospheric variables are listed  
 293 separately.

294

295 Table 3 Bias of ice thickness, snow depth, and bias ratio for each forcing variable come from Table  
 296 2. ‘All’ means using the full set of ERA5 atmospheric forcing.

Variable	Bias		Bias ratio (%)
	Ice (cm)	Snow (cm)	Forcing
$R_{sd}$ ( $\text{W m}^{-2}$ )	-0.044	-0.130	9.031
$R_{ld}$ ( $\text{W m}^{-2}$ )	3.050	2.243	-9.672
$T_a$ (K)	0.001	0.029	-0.453
$Q_a$ ( $10^{-4} \text{ kg kg}^{-1}$ )	1.099	-1.299	-9.326
$P$ ( $\text{mm day}^{-1}$ )	14.519	17.312	303.509
$\Theta_a$ (K)	-0.483	0.407	0.112
$\rho_a$ ( $\text{kg m}^{-3}$ )	0.119	-0.071	-1.592
$U_a$ ( $\text{m s}^{-1}$ )	-0.311	-3.421	50.735
<i>All</i>	16.824	17.882	/

297

298 To determine the sensitivity of sea ice and snow depth near Zhongshan station on atmospheric  
 299 forcing, we designed a set of numerical experiments named SEN2. In the control run, the forcing of  
 300 the simulation directly used the means of observed atmospheric variables (Mean\_Obs in Table 4).  
 301 For a specific atmospheric variable, we build a set of sensitive runs. The focused atmospheric

302 variable changed from its mean (Range in Table 4), and other variables are the same as the control  
 303 run. Considering the actual range of each observed variable on an interannual scale (Van Den Broeke  
 304 et al., 2004; Jakobs et al., 2020; Roussel et al., 2020), we set the maximum change in  $T_a$ ,  $\Theta_a$  and  $\rho_a$   
 305 to 2%, and other atmospheric variables to 50%. Then, we concluded the sensitivity of sea ice and  
 306 snow to each atmospheric forcing from its corresponding sensitive runs. Because sea ice and snow  
 307 depth show a quasi-linear response to the change in each specific atmospheric forcing (not shown),  
 308 the choice of the variable's range will not alter the sensitivity results.

309

310 Table 4 The atmospheric forcing (Mean\_obs for the control run and range for the sensitive run), and  
 311 sensitivity from SEN2.

Variable	Mean_Obs (Control)	Range (%)	Sensitivity	
			Ice (cm/%)	Snow (cm/%)
$R_{sd}$ (W m <sup>-2</sup> )	67.714	±50	-0.033	-0.008
$R_{ld}$ (W m <sup>-2</sup> )	198.023	±50	-0.368	-0.201
$T_a$ (K)	257.809	±2	-1.247	-0.526
$Q_a$ (10 <sup>-4</sup> kg kg <sup>-1</sup> )	8.247	±50	-0.025	0.029
$P$ (mm day <sup>-1</sup> )	0.660	±50	-0.032	0.135
$\Theta_a$ (K)	259.437	±2	-1.297	-0.491
$\rho_a$ (kg m <sup>-3</sup> )	1.322	±2	-0.054	0.021
$U_a$ (m s <sup>-1</sup> )	4.228	±50	-0.054	-0.022

312

313 Comparing the individual biases in Table 3, it turns out that  $P$  and  $R_{ld}$  from ERA5 contribute to  
 314 the bias in sea ice thickness most strongly. For snow depth,  $P$ ,  $U_a$ , and  $R_{ld}$  contribute the largest. In  
 315 Table 4, the sensitivity of ice thickness and snow depth to each atmospheric variable are listed.  
 316 Comparing the individual sensitivity, it turns out that the sea ice thickness and snow depth are most  
 317 sensitive to  $T_a$  and  $\Theta_a$ . However,  $T_a$  from ERA5 is close to the *in situ* observation, so the simulated  
 318 sea ice thickness and snow depth are hardly impacted (Table 3). The results from SEN1 reveal that  
 319 the overestimation in  $P$  in ERA5 is the primary source of the overestimation of sea ice thickness  
 320 and snow depth, even with less sensitivity to precipitation (Table 4).

321 To clarify the effect of specific forcing further, we replaced the  $x$  forcing in Sim\_Obs with the  
 322 corresponding ERA5 variable and named it Sim\_ERA\_x. Compared with Sim\_Obs, Sim\_ERA\_P  
 323 overestimates the snow depth since May (Figure 4b) and shows a significant positive bias in sea ice

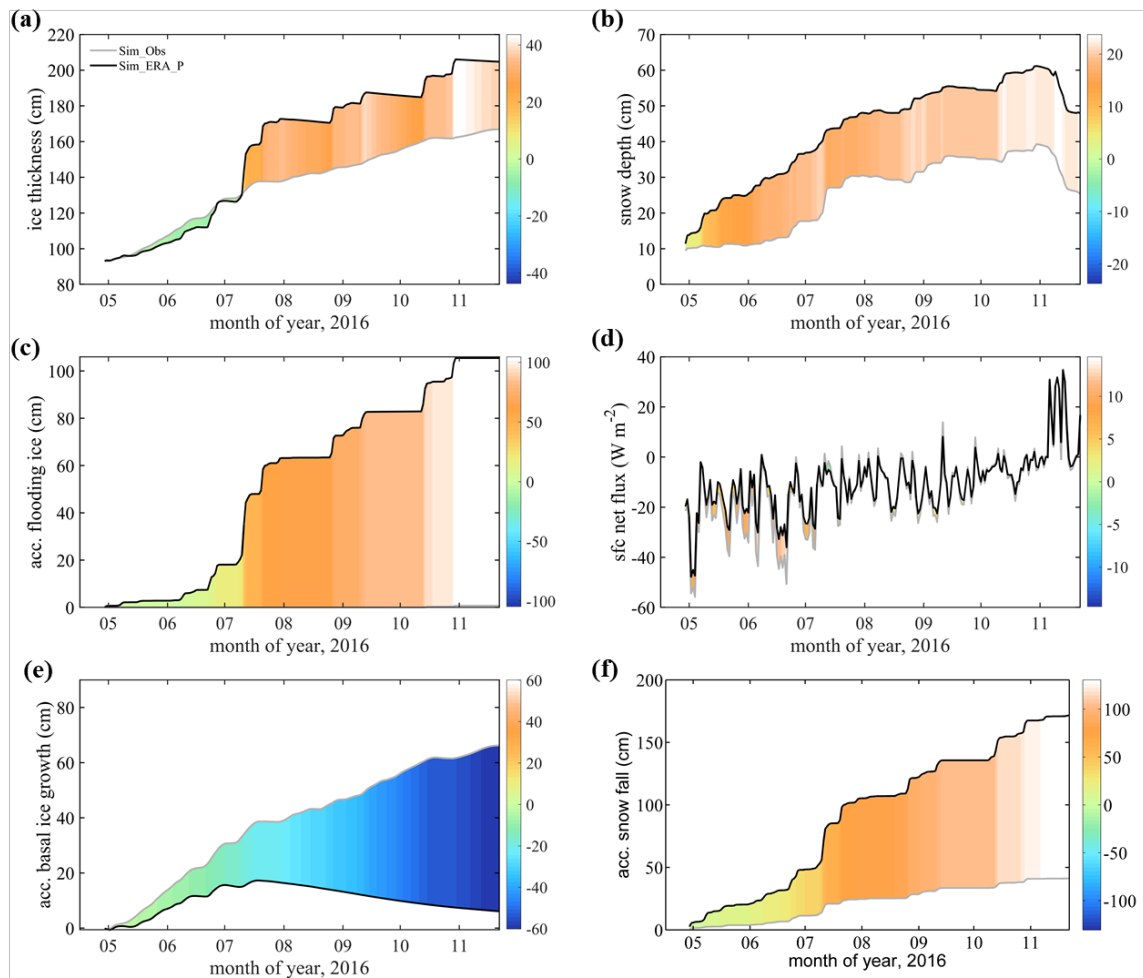
324 thickness after July 11 (Figure 4a). Before July 11, the sea ice thickness from Sim\_ERA\_P was even  
325 smaller than that from Sim\_Obs.

326 To find out why the snow and sea ice behaves differently, we first investigate the net heat flux  
327 into the snow surface  $H_N$  (positive downward):

$$328 \quad H_N = Rn + Hs + Hl, (2)$$

329 where  $Rn$ ,  $Hs$ , and  $Hl$  are the net surface radiation flux, the sensible heat flux, and the latent heat  
330 flux, respectively. All energy fluxes are defined as positive downward. Because the simulated snow  
331 layer in SIM\_ERA\_P is much deeper than in SIM\_Obs, the difference in  $H_N$  reflects the modification  
332 of the surface energy flux due to the changed snow layer. From Figure 4d, it can be deduced that the  
333 overestimation of snow depth in SIM\_ERA\_P results in a positive anomaly of  $H_N$  before July 11,  
334 which hampers the sea ice growth. Later the difference in  $H_N$  becomes relatively small. The  
335 dependence of  $H_N$  on the snow depth is significant when the snow layer is shallow (<20 cm in this  
336 study). If the snow layer is deep enough, its impact on the net surface heat flux ceases.

337 After July 11, the difference in sea ice thickness between the two simulations increases quickly  
338 from ~0 to >40 cm (Figure 4a). We attribute that to flooding with subsequent snow-ice formation  
339 (Powell and others, 2005). The continuously deepening snow layer reduces the sea ice freeboard.  
340 When heavy snowfall occurs, which frequently happens after July 11, the snow load pushes the sea  
341 ice surface below sea level, and seawater floods onto the sea ice surface, causing the overlying snow  
342 to freeze. This snow-ice formation process will form flooding ice (snow-ice thickness) at the sea ice  
343 surface and rapidly increase the total sea ice thickness (Figure 4a). The difference (~100 cm) in  
344 accumulated flooding ice (Figure 4c) between Sim\_Obs (0.8 cm) and Sim\_ERA\_P (105.5 cm) is  
345 much greater than the difference (~40 cm) in simulated sea ice thickness (Figure 4a), while the net  
346 surface heat flux compares well after July 11 (Figure 4d). This difference may be because as the  
347 snow-ice process occurs, the increase in sea ice thickness will reduce the heat loss from the ice cover  
348 and inhibit the basal growth of sea ice in winter (Figure 4e). The flooding-induced snow-ice  
349 formation happens at a rate larger than 0.5 cm per hour after July 11. The snowfall (Figure 2b) is  
350 converted to new snow depth at the top surface (Figure 4f) using a snow density of 330 kg m<sup>-3</sup> in  
351 ICEPACK (Hunke et al., 2019). Comparing Figure 4b with Figure 4f, we find that the change in  
352 actual snow depth (11 cm) is much lower than the expected accumulated snowfall (57 cm),  
353 indicating that the flooding process reduces about four-fifths of snow depth over sea ice.



355

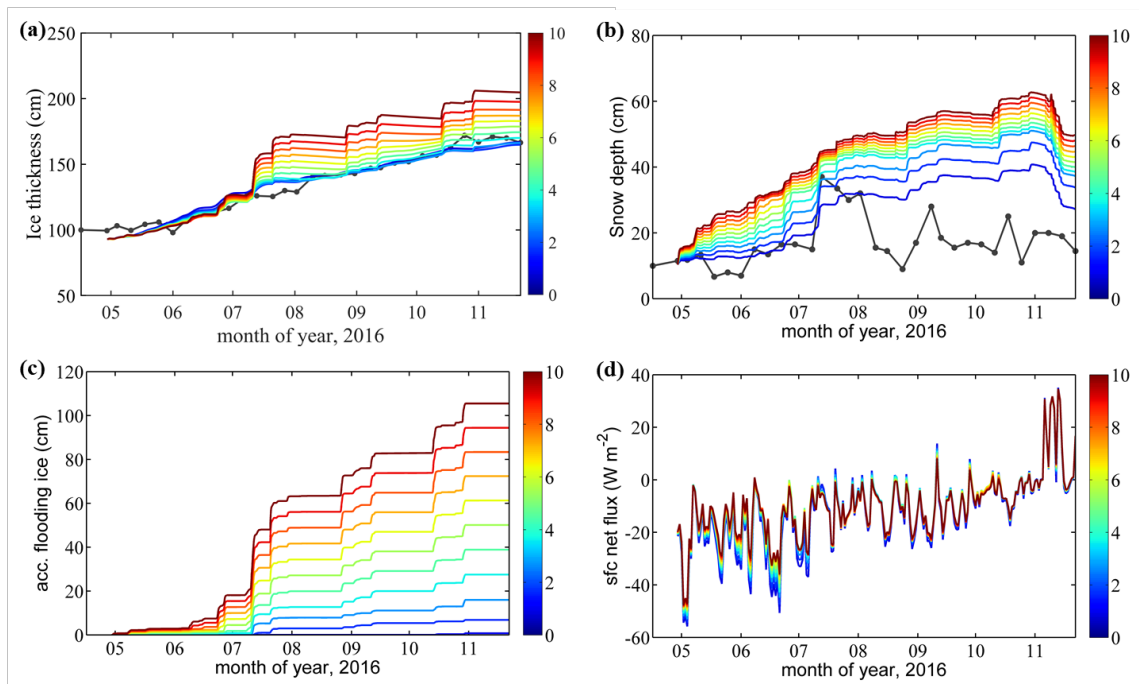
356 Figure 4 Times series of (a) sea ice thickness, (b) snow depth, (c) accumulated flooding ice, (d) net  
 357 surface heat flux, (e) accumulated basal ice growth, and (f) accumulated snowfall. The gray line  
 358 represents the simulation using precipitation from observation (Sim\_Obs). The black line represents  
 359 the simulation using precipitation from ERA5 (Sim\_ERA\_P). The color bar represents their  
 360 difference (Sim\_ERA\_P – Sim\_Obs).

361

### 3.5 Additional sensitivity simulations on the precipitation bias

362

The precipitation from ERA5 shows the most significant deviation compared to the *in situ*  
 363 observation and contributes the largest to the sea ice and snow simulation bias. To determine the  
 364 cause of differences in the sea ice and snow response to precipitation, we set up ten sensitivity  
 365 experiments named SEN3 (Figure 5). In the  $n$ -th experiment,  $n \times 10\%$  of the daily difference between  
 366  $P$  from ERA5 and the *in situ* observation is added to the observed  $P$  on that day. This procedure  
 367 gradually increases the magnitude of the precipitation in the experiments while the timing of the  
 368 daily precipitation events remains almost unchanged.



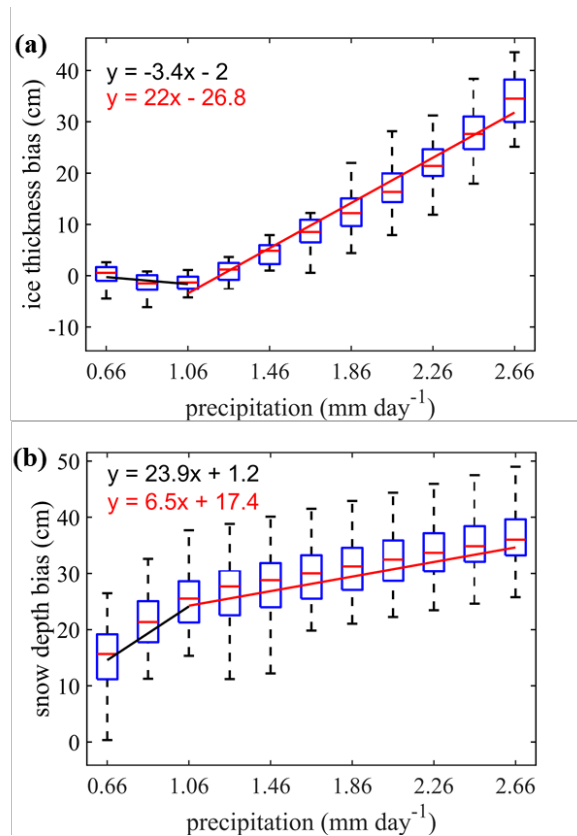
370

371 Figure 5 Time series of the simulated (a) sea ice thickness, (b) snow depth, (c) accumulated flooding  
 372 ice, and (d) net surface heat flux in the  $n$  experiments of SEN3. The black solid point lines show the  
 373 *in situ* observations (Obs). The 11 colored lines denote the 11 sensitivity experiments. When  $n = 0$ ,  
 374 precipitation is from the *in situ* observation. When  $n = 10$ , precipitation is from ERA5.

375

376





377

378 Figure 6 Box plot of simulation bias (simulation minus observation) of (a) sea ice thickness and (b)  
 379 snow depth over the daily mean precipitation in the different sensitivity experiments (n increases  
 380 from left to right). On the x-axis, 0.66 mm refers to the experiment with n=0 (*in situ* precipitation),  
 381 and 2.66 mm refers to the n=10 experiment (ERA5 precipitation). Two linear regression lines (black  
 382 and red) are derived for  $x \leq 1.06$  mm and  $x > 1.06$  mm based on the mean of ice thickness and  
 383 snow depth.

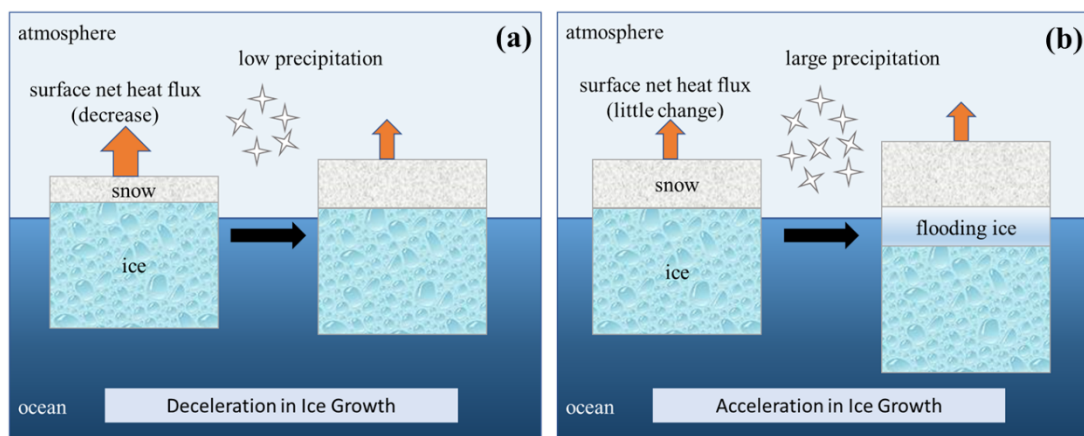
384 We define the bias as the difference between simulations and observations from July 27 to the  
 385 end of November. Different start or end dates of this period do not change this result. The bias of  
 386 both sea ice thickness and snow depth linearly grows with increasing precipitation (Figure 6). The  
 387 simulation bias of the sea ice thickness is relatively small before the precipitation increases by about  
 388 1 mm per day. We suggested that the snow-ice formation is small (Figure 5c), and the insulation of  
 389 the snow layer (Figure 5d) hampers the sea ice growth. In fact, the simulated sea ice thickness even  
 390 decreases (at a rate of  $-3.4$  cm/(mm day<sup>-1</sup>)) when the added precipitation is  $< 1$  mm day<sup>-1</sup>. When the  
 391 added precipitation is  $> 1$  mm day<sup>-1</sup>, the simulated sea ice thickness quickly increases at a rate of 22  
 392 cm/(mm day<sup>-1</sup>).

393 In contrast, the simulated snow depth increases rapidly at 23.9 cm/(mm day<sup>-1</sup>) when the enforced

394 precipitation remains small but at a rate of 6.5 cm when the added precipitation is large. This is  
 395 because more snow is converted into flooding ice, and the snow-ice formation process strongly  
 396 overrules the larger insulation effect from the snow layer, promoting sea ice growth.

397 The snow-ice process is based on Archimedes' Principle. Therefore, the threshold value (1  
 398 mm/day<sup>-1</sup>) is related to the density value of ice, snow, and water in model parameterization as well  
 399 as the sea ice thickness and snow depth. If sea ice and snow density, initial snow depth decrease, or  
 400 seawater density and initial ice thickness increase, the threshold will increase, and vice versa. These  
 401 different effects of increases in precipitation on the snow and sea ice growth are illustrated in Figure  
 402 7, emphasizing the role of flooding via snow-ice formation. When the snow layer is shallow,  
 403 increases in precipitation will quickly deepen the snow layer and inhibit the growth of sea ice  
 404 thickness due to the insulation of snow. The decrease in the surface net heat flux is the dominant  
 405 factor. While the snow layer is deep and large precipitation is present, the flooding process induces  
 406 snow-ice formation, and the sea ice grows quickly while the snow depth increases only slowly.

407



408

409 Figure 7 Schematic diagram for (a) low precipitation and (b) large precipitation events illustrating  
 410 the precipitation effect on sea ice growth. The orange arrows represent surface net heat flux, and  
 411 different colored boxes indicate the layer of snow, flooding ice, and sea ice.

412

#### 413 4 Shortcomings

414 The simulated ice thickness and snow depth deviate from the observations in this study (Figure  
 415 3). We list the shortcomings that could affect the simulation: 1) Superimposed ice is not considered  
 416 in this study; 2) The snow-ice formation might be overestimated on the landfast sea ice in ICEPACK;  
 417 3) The snowdrift process has not been involved in the version of ICEPACK used here.

418 Superimposed ice is present in early autumn when the snow starts to melt (Kawamura et al.,  
419 1997) and contributes significantly to sea ice growth (up to 20% of mass) (Granskog et al., 2004).  
420 Superimposed ice usually corresponds to liquid precipitation or melted snow that permeates  
421 downward to form a fresh slush layer and refreezes. The superimposed ice is implemented in  
422 ICEPACK via the melt ponds parametrization but has not been considered in this study. Therefore,  
423 the simulation may underestimate sea ice thickness and overestimate snow depth compared to the  
424 observation in November (Figure 3a). We will apply the melt ponds scheme in the follow-up  
425 research work.

426 Flooding-induced snow-ice formation is common in the Antarctic ocean because of the thin ice  
427 and heavy snowfall (Kawamura et al., 1997). It can contribute to considerable ice mass (12%-36%)  
428 and reduce the snow depth by up to 42-70%, depending on the season and location (Jeffries et al.,  
429 2001). The parameterization of the flooding process in the ICEPACK is based on Archimedes'  
430 Principle for the pack ice, which might be problematic for the coastal landfast sea ice. With a much  
431 larger volume and shallower seawater around than the pack sea ice, part of the coastal landfast sea  
432 ice might contact the sea bed rather than float in the sea. Thus, the flooding should be much weaker  
433 even with weighted snow cover. Besides, the change in density of ice due to the flooding process is  
434 significant (Saloranta, 2000) but not well considered in ICEPACK. For example, a slushy layer of  
435 10 cm depth would refreeze within three days from observation (Provost et al., 2017), while the  
436 process only needs one day in ICEPACK. Hence, the landfast sea ice growth due to snow-ice  
437 formation needs improvement in ICEPACK, especially when the input precipitation is significantly  
438 exaggerated, e.g., the ERA5 forcing.

439 Surface drifting snow particles play an essential role in the surface mass balance (Van den  
440 Broeke et al., 2004). Figure 3b shows that the observed snow depth has quickly decreased from 32  
441 cm on August 2 to 15.5cm on August 10, which should be attributed to the snowdrift because the  
442 surface wind is  $> 8 \text{ m s}^{-1}$  in most of this period (Figure 2c). Friction velocity becomes sufficiently  
443 high to overcome the gravity and bonds between snow particles in this strong wind and raise the  
444 snow particles from the surface (van den Broeke et al., 2006; Thiery et al., 2012; Tanji et al., 2021).  
445 However, the mean surface wind in ERA5 is convergent around the observation site during the  
446 intense wind period (Figure 8), which might not be expected for snow depth to decrease due to  
447 snowdrift. The coarse resolution of the atmospheric reanalysis might not produce a realistic surface

448 wind field, which is primarily determined by the local topography (Van Den Broeke et al., 1999;  
449 Frezzotti et al., 2005). In addition, surface sublimation of drifting snow particles, which is most  
450 significant in warm, dry, and windy weather (Thiery et al., 2012), plays an important role in surface  
451 mass balance (Van den Broeke et al., 2004) but has not been involved in ICEPACK yet.

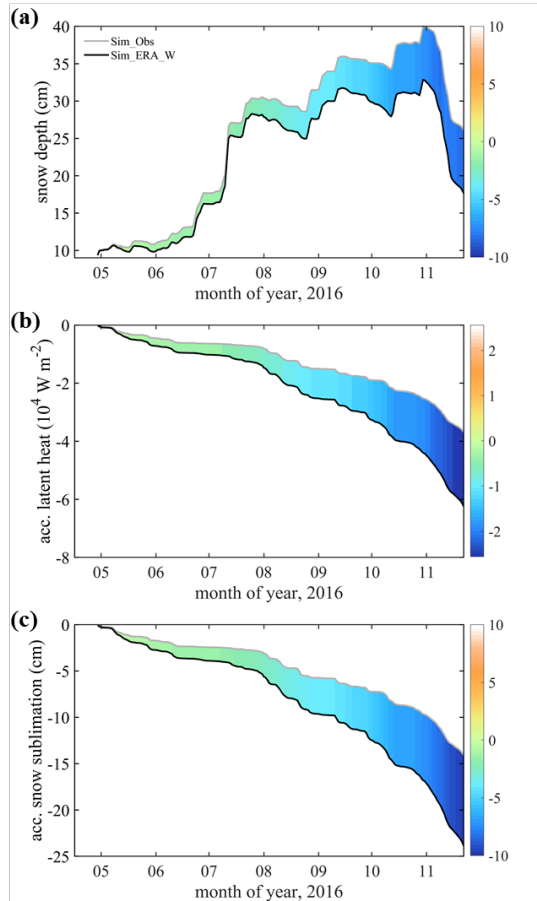
452  
453 Figure 8 The mean ERA5 surface wind and divergence from August 2 to 10. The black line  
454 represents the coastline, and the red point represents the observation site.

455

## 456 **5 Discussions**

457 The surface wind can affect the snow depth by changing the surface heat fluxes (Fairall et al.,  
458 2003). Compared with Sim\_Obs, Sim\_ERA\_W gives a  $-2.5 \times 10^4 \text{ W m}^{-2}$  lower latent heat flux  
459 (positive downward) on average (Figure 9b), i.e., a larger sublimation (Figure 9c), and a reduction  
460 of about -3.4 cm of the snow depth (Figure 9a). Therefore, the overestimation in the surface wind  
461 from ERA5 partly neutralizes the effect of overestimated precipitation.

462



463

464 Figure 9 Times series of (a) snow depth, (b) accumulated latent heat flux, and (c) accumulated snow  
 465 sublimation. The gray line represents the simulation using wind from the observation (Sim\_Obs).  
 466 The black line represents the simulation using wind from ERA5 (Sim\_ERA\_W). The color bar  
 467 represents their difference (Sim\_ERA\_W – Sim\_Obs).

468 The oceanic forcing also plays an essential role in sea ice evolution (Uotila et al., 2019). Heat  
 469 flux from the ocean boundary layer changes the sea ice energy balance (Maykut and Untersteiner,  
 470 1971). The ocean heat flux is mainly impacted by summer insolation through open leads, thin ice,  
 471 melt ponds (Perovich and Maykut, 1990), and upward heat transfer through vertical turbulent  
 472 mixing (McPhee et al., 1999). Because the oceanic observations under sea ice are challenging, most  
 473 sea ice models directly use some empirical values, like the default value in CCSM3, to build the  
 474 ocean boundary condition (e.g., Yang et al., 2016b; Turner and Hunke, 2015). Although some  
 475 oceanic variables, like the water temperature and salinity, are from observation, others refer to  
 476 previous studies, like the mixed layer depth. The uncertainty in oceanic forcing might be as  
 477 important as the atmospheric ones, which will be focused on in our coming work.

478

## 479 **6 Conclusions**

480 This work uses the single-column sea ice model ICEPACK forced by the ERA5 atmospheric  
481 reanalysis and atmospheric *in situ* observations to simulate snow depth and sea ice thickness at  
482 Zhongshan Station, Antarctic. We find that forced by atmospheric variables from *in situ* observations.  
483 The ICEPACK can reasonably simulate the sea ice thickness evolution but significantly  
484 overestimates the snow depth after the heavy snowfall on July 11. When using atmospheric forcing  
485 from ERA5, sea ice thickness simulation is close to observation before July 11 but suddenly  
486 increases after the snowfall event.

487 From the sensitivity experiments, we find that the significant deviation in the precipitation of  
488 ERA5 contribute to the largest bias in both sea ice thickness and snow depth even though the  
489 precipitation is moderately sensitive to sea ice thickness (-0.032 cm/%) and snow depth (0.135  
490 cm/%). On average, about 2 mm day<sup>-1</sup> more precipitation in ERA5 is found during the observation  
491 period, which produces about 14.5 cm excess in sea ice thickness and 17.3 cm more snow depth.

492 We further explore the physical mechanism of the effect of precipitation on ice thickness. Snow-  
493 ice formation can be triggered by a heavy snowfall episode, like on July 11. It efficiently produces  
494 ice at the sea ice surface, decelerates the snow accumulation, and inhibits sea ice's basal growth.  
495 When the snowfall is weak, the snow layer thickens quickly and hampers the sea ice growth through  
496 its insulation effect. When the snowfall increases to a certain degree (~1 mm day<sup>-1</sup>), it will trigger a  
497 continuous flooding process, accelerating the sea ice growth and slowing down the snow layer  
498 thickening.

499

## 500 **Acknowledgments**

501 The authors would like to thank ECMWF for the ERA5 reanalysis data set and the Russian  
502 meteorological station Progress II for the precipitation observations. We are grateful to CICE  
503 Consortium for sharing ICEPACK and its documentation ([https://github.com/CICE-  
504 Consortium/Icepack](https://github.com/CICE-Consortium/Icepack)). This study is supported by the National Natural Science Foundation of China  
505 (No. 41941009, 41922044), the Guangdong Basic and Applied Basic Research Foundation (No.  
506 2020B1515020025), the Southern Marine Science and Engineering Guangdong Laboratory (Zhuhai)  
507 (No. SML2020SP007), and CAS "Light of West China" Program (No. E129030101, Y929641001).  
508 PH was supported by AAS grant 4506.

## 509 **References**

510 Barthélemy, A., Goosse, H., Fichet, T., and Lecomte, O.: On the sensitivity of Antarctic sea ice model  
511 biases to atmospheric forcing uncertainties, *Clim. Dynam.*, 51, 1585-1603, 2018.

512 Bitz, C. M., Holland, M. M., Weaver, A. J., and Eby, M.: Simulating the ice - thickness distribution in a  
513 coupled climate model, *Journal of Geophysical Research: Oceans*, 106, 2441-2463, 2001.

514 Bracegirdle, T. J., and Marshall, G. J.: The reliability of Antarctic tropospheric pressure and temperature  
515 in the latest global reanalyses, *J. Climate*, 25, 7138-7146, 2012.

516 Briegleb, B. P., and Light, B.: A Delta-Eddington multiple scattering parameterization for solar radiation  
517 in the sea ice component of the Community Climate System Model, NCAR Tech. Note NCAR/TN-472+  
518 STR, 1-108, 2007.

519 Bromwich, D. H., Fogt, R. L., Hodges, K. I., and Walsh, J. E.: A tropospheric assessment of the ERA -  
520 40, NCEP, and JRA - 25 global reanalyses in the polar regions, *Journal of Geophysical Research: At-*  
521 *mospheres*, 112, D10111, 2007.

522 Chemke, R., and Polvani, L. M.: Using multiple large ensembles to elucidate the discrepancy between  
523 the 1979 - 2019 modeled and observed Antarctic sea ice trends, *Geophys. Res. Lett.*, 47, e2020G-  
524 e88339G, 2020.

525 Cheng, B., Mäkynen, M., Similä, M., Rontu, L., and Vihma, T.: Modelling snow and ice thickness in the  
526 coastal Kara Sea, Russian Arctic, *Ann. Glaciol.*, 54, 105-113, 2013.

527 Cheng, B., Zhang, Z., Vihma, T., Johansson, M., Bian, L., Li, Z., and Wu, H.: Model experiments on  
528 snow and ice thermodynamics in the Arctic Ocean with CHINARE 2003 data, *Journal of Geophysical*  
529 *Research: Oceans*, 113, C9020, 2008.

530 Collins, W. D., Bitz, C. M., Blackmon, M. L., Bonan, G. B., Bretherton, C. S., Carton, J. A., Chang, P.,  
531 Doney, S. C., Hack, J. J., and Henderson, T. B.: The community climate system model version 3  
532 (CCSM3), *J. Climate*, 19, 2122-2143, 2006.

533 Fairall, C. W., Bradley, E. F., Hare, J. E., Grachev, A. A., and Edson, J. B.: Bulk parameterization of air-  
534 sea fluxes: Updates and verification for the COARE algorithm, *J. Climate*, 16, 571-591, 2003.

535 Fréville, H., Brun, E., Picard, G., Tatarinova, N., Arnaud, L., Lanconelli, C., Reijmer, C., and Van den  
536 Broeke, M.: Using MODIS land surface temperatures and the Crocus snow model to understand the  
537 warm bias of ERA-Interim reanalyses at the surface in Antarctica, *The Cryosphere*, 8, 1361-1373, 2014.

538 Frezzotti, M., Pourchet, M., Flora, O., Gandolfi, S., Gay, M., Urbini, S., Vincent, C., Becagli, S., Grag-  
539 nani, R., and Proposito, M.: Spatial and temporal variability of snow accumulation in East Antarctica  
540 from traverse data, *J. Glaciol.*, 51, 113-124, 2005.

541 Gascoïn, S., Lhermitte, S., Kinnard, C., Bortels, K., and Liston, G. E.: Wind effects on snow cover in  
542 Pascua-Lama, Dry Andes of Chile, *Adv. Water Resour.*, 55, 25-39, 2013.

543 Granskog, M. A., Leppäranta, M., Kawamura, T., Ehn, J., and Shirasawa, K.: Seasonal development of  
544 the properties and composition of landfast sea ice in the Gulf of Finland, the Baltic Sea, *Journal of Geo-*  
545 *physical Research: Oceans*, 109, 10.1029/2003JC001874, 2004.

546 Hao, G., Pirazzini, R., Yang, Q., Tian, Z., and Liu, C.: Spectral albedo of coastal landfast sea ice in Prydz  
547 Bay, Antarctica, *J. Glaciol.*, 67, 1-11, 2020.

548 Hao, G., Yang, Q., Zhao, J., Deng, X., Yang, Y., Duan, P., Zhang, L., Li, C., and Cui, L.: Observation  
549 and analysis of landfast ice surrounding Zhongshan Station, Antarctic in 2016, *Haiyang Xuebao*, 9, 26-39,  
550 2019.

551 Heil, P.: Atmospheric conditions and fast ice at Davis, East Antarctica: A case study, *Journal of Geo-*  
552 *physical Research: Oceans*, 111, C5009, 2006.

553 Heil, P., Allison, I., and Lytle, V. I.: Seasonal and interannual variations of the oceanic heat flux under a  
554 landfast Antarctic sea ice cover, *Journal of Geophysical Research: Oceans*, 101, 25741-25752, 1996.

555 Hersbach, H., Bell, B., Berrisford, P., Hirahara, S., Horányi, A., Muñoz Sabater, J., Nicolas, J., Peubey,

556 C., Radu, R., and Schepers, D.: The ERA5 global reanalysis, *Q. J. Roy. Meteor. Soc.*, 146, 1999-2049,  
557 2020.

558 Hersbach, H., and Dee, D.: ERA5 reanalysis is in production, *ECMWF Newsletter* 147, Reading, UK:  
559 ECMWF. [Retrieved from <https://www.ecmwf.int/en/newsletter/147/news/era5-reanalysis-production>],  
560 2016.

561 Hunke, E., Allard, R., Bailey, D. A., Blain, P., Craig, T., Dupont, F., DuVivier, A., Grumbine, R., Hebert,  
562 D., Holland, M., Jeffery, N., Lemieux, J., Rasmussen, T., Ribergaard, M., Roberts, A., Turner, M., and  
563 Winton, M.: CICE-Consortium/Icepack: Icepack1.1.1, doi:10.5281/zenodo.3251032, 2019.

564 Jakobs, C. L., Reijmer, C. H., Smeets, C. P., Trusel, L. D., Van De Berg, W. J., Van Den Broeke, M. R.,  
565 and Van Wessem, J. M.: A benchmark dataset of in situ Antarctic surface melt rates and energy balance,  
566 *J. Glaciol.*, 66, 291-302, 2020.

567 Jeffries, M. O., Krouse, H. R., Hurst-Cushing, B., and Maksym, T.: Snow-ice accretion and snow-cover  
568 depletion on Antarctic first-year sea-ice floes, *Ann. Glaciol.*, 33, 51-60, DOI:  
569 10.3189/172756401781818266, 2001.

570 Jones, R. W., Renfrew, I. A., Orr, A., Webber, B., Holland, D. M., and Lazzara, M. A.: Evaluation of  
571 four global reanalysis products using in situ observations in the Amundsen Sea Embayment, Antarctica,  
572 *Journal of Geophysical Research: Atmospheres*, 121, 6240-6257, 2016.

573 Kawamura, T., Ohshima, K. I., Takizawa, T., and Ushio, S.: Physical, structural, and isotopic character-  
574 istics and growth processes of fast sea ice in Lützow-Holm Bay, Antarctica, *Journal of Geophysical*  
575 *Research: Oceans*, 102, 3345-3355, 10.1029/96JC03206, 1997.

576 Krumpen, T., Birrien, F., Kauker, F., Rackow, T., Albedyll, L. V., Angelopoulos, M., Belter, H. J., Bes-  
577 sonov, V., Damm, E., and Dethloff, K.: The MOSAiC ice floe: sediment-laden survivor from the Siberian  
578 shelf, *The Cryosphere*, 14, 2173-2187, 2020.

579 Lei, R., Li, Z., Cheng, B., Zhang, Z., and Heil, P.: Annual cycle of landfast sea ice in Prydz Bay, east  
580 Antarctica, *Journal of Geophysical Research: Oceans*, 115, C2006, 2010.

581 Leppäranta, M.: A growth model for black ice, snow ice and snow thickness in subarctic basins, *Hydrology*  
582 *Research*, 14, 59-70, 1983.

583 Lindsay, R., Wensnahan, M., Schweiger, A., and Zhang, J.: Evaluation of seven different atmospheric  
584 reanalysis products in the Arctic, *J. Climate*, 27, 2588-2606, 2014.

585 Lindsay, R., and Schweiger, A.: Arctic sea ice thickness loss determined using subsurface, aircraft, and  
586 satellite observations, *The Cryosphere*, 9, 269-283, 2015.

587 Liston, G. E., Polashenski, C., Rösel, A., Itkin, P., King, J., Merkouriadi, I., and Haapala, J.: A distributed  
588 snow - evolution model for sea - ice applications (SnowModel), *Journal of Geophysical Research:*  
589 *Oceans*, 123, 3786-3810, 2018.

590 Liu, C., Gao, Z., Yang, Q., Han, B., Wang, H., Hao, G., Zhao, J., Yu, L., Wang, L., and Li, Y.: Measure-  
591 ments of turbulence transfer in the near-surface layer over the Antarctic sea-ice surface from April  
592 through November in 2016, *Ann. Glaciol.*, 61, 12-23, 2020.

593 Liu, C., Hao, G., Li, Y., Zhao, J., Lei, R., Cheng, B., Gao, Z., and Yang, Q.: The sensitivity of parame-  
594 terization schemes in thermodynamic modeling of the landfast sea ice in Prydz Bay, East Antarctica, *J.*  
595 *Glaciol.*, 1-16, 2022.

596 Massom, R. A., Eicken, H., Hass, C., Jeffries, M. O., Drinkwater, M. R., Sturm, M., Worby, A. P., Wu,  
597 X., Lytle, V. I., and Ushio, S.: Snow on Antarctic sea ice, *Rev. Geophys.*, 39, 413-445, 2001.

598 Massonnet, F., Fichet, T., Goosse, H., Vancoppenolle, M., Mathiot, P., and König Beatty, C.: On the  
599 influence of model physics on simulations of Arctic and Antarctic sea ice, *The Cryosphere*, 5, 687-699,



600 2011.

601 Maykut, G. A., and Untersteiner, N.: Some results from a time-dependent thermodynamic model of sea  
602 ice, *Journal of Geophysical Research (1896-1977)*, 76, 1550-1575, 10.1029/JC076i006p01550, 1971.

603 Maykut, G. A., and McPhee, M. G.: Solar heating of the Arctic mixed layer, *Journal of Geophysical*  
604 *Research: Oceans*, 100, 24691-24703, 1995.

605 McPhee, M. G., Kottmeier, C., and Morison, J. H.: Ocean Heat Flux in the Central Weddell Sea during  
606 Winter, *J. Phys. Oceanogr.*, 29, 1166-1179, 10.1175/1520-0485(1999)029<1166:OHFITC>2.0.CO;2,  
607 1999.

608 Merkouriadi, I., Liston, G. E., Graham, R. M., and Granskog, M. A.: Quantifying the potential for snow -  
609 ice formation in the Arctic Ocean, *Geophys. Res. Lett.*, 47, e2019G-e85020G, 2020.

610 Parkinson, C. L.: A 40-y record reveals gradual Antarctic sea ice increases followed by decreases at rates  
611 far exceeding the rates seen in the Arctic, *Proceedings of the National Academy of Sciences*, 116, 14414-  
612 14423, 2019.

613 Parkinson, C. L., and Cavalieri, D. J.: Antarctic sea ice variability and trends, 1979-2010, *The Cryosphere*,  
614 6, 871-880, 2012.

615 Perovich, D. K., and Maykut, G. A.: Solar heating of a stratified ocean in the presence of a static ice  
616 cover, *Journal of Geophysical Research: Oceans*, 95, 18233-18245, 10.1029/JC095iC10p18233, 1990.

617 Provost, C., Sennéchaël, N., Miguet, J., Itkin, P., Rösel, A., Koenig, Z., Villaceros Robineau, N., and  
618 Granskog, M. A.: Observations of flooding and snow - ice formation in a thinner Arctic sea - ice regime  
619 during the N - ICE2015 campaign: Influence of basal ice melt and storms, *Journal of Geophysical Re-*  
620 *search: Oceans*, 122, 7115-7134, 2017.

621 Roussel, M., Lemonnier, F., Genthon, C., and Krinner, G.: Brief communication: Evaluating Antarctic  
622 precipitation in ERA5 and CMIP6 against CloudSat observations, *The Cryosphere*, 14, 2715-2727, 2020.

623 Saloranta, T. M.: Modeling the evolution of snow, snow ice and ice in the Baltic Sea, *Tellus A: Dynamic*  
624 *Meteorology and Oceanography*, 52, 93-108, 2000.

625 Schlosser, E., Haumann, F. A., and Raphael, M. N.: Atmospheric influences on the anomalous 2016  
626 Antarctic sea ice decay, *The Cryosphere*, 12, 1103-1119, 2018.

627 Stroeve, J. C., Serreze, M. C., Holland, M. M., Kay, J. E., Malanik, J., and Barrett, A. P.: The Arctic' s  
628 rapidly shrinking sea ice cover: a research synthesis, *Climatic Change*, 110, 1005-1027, 2012.

629 Stuecker, M. F., Bitz, C. M., and Armour, K. C.: Conditions leading to the unprecedented low Antarctic  
630 sea ice extent during the 2016 austral spring season, *Geophys. Res. Lett.*, 44, 9008-9019, 2017.

631 Tanji, S., Inatsu, M., and Okaze, T.: Development of a snowdrift model with the lattice Boltzmann  
632 method, *Progress in Earth and Planetary Science*, 8, 1-16, 2021.

633 Tetzner, D., Thomas, E., and Allen, C.: A Validation of ERA5 Reanalysis Data in the Southern Antarctic  
634 Peninsula—Ellsworth Land Region, and Its Implications for Ice Core Studies, *Geosciences*, 9, 289, 2019.

635 Thiery, W., Gorodetskaya, I. V., Bintanja, R., Van Lipzig, N., Van den Broeke, M. R., Reijmer, C. H.,  
636 and Kuipers Munneke, P.: Surface and snowdrift sublimation at Princess Elisabeth station, East Antarc-  
637 tica, *The Cryosphere*, 6, 841-857, 2012.

638 Tsamados, M., Feltham, D. L., and Wilchinsky, A. V.: Impact of a new anisotropic rheology on simula-  
639 tions of Arctic sea ice, *Journal of Geophysical Research: Oceans*, 118, 91-107, 2013.

640 Turner, A. K., Hunke, E. C., and Bitz, C. M.: Two modes of sea-ice gravity drainage: A parameterization  
641 for large - scale modeling, *Journal of Geophysical Research: Oceans*, 118, 2279-2294, 2013.

642 Turner, A. K., and Hunke, E. C.: Impacts of a mushy-layer thermodynamic approach in global sea-ice  
643 simulations using the CICE sea-ice model, *Journal of Geophysical Research: Oceans*, 120, 1253-1275,

644 2015.

645 Turner, J., Phillips, T., Marshall, G. J., Hosking, J. S., Pope, J. O., Bracegirdle, T. J., and Deb, P.: Un-  
646 precedented springtime retreat of Antarctic sea ice in 2016, *Geophys. Res. Lett.*, 44, 6868-6875,  
647 2017.

648 Uotila, P., Goosse, H., Haines, K., Chevallier, M., Barthélemy, A., Bricaud, C., Carton, J., Fučkar,  
649 N., Garric, G., and Iovino, D.: An assessment of ten ocean reanalyses in the polar regions, *Clim. Dynam.*,  
650 52, 1613-1650, 2019.

651 Urraca, R., Huld, T., Gracia-Amillo, A., Martinez-de-Pison, F. J., Kaspar, F., and Sanz-Garcia, A.: Eval-  
652 uation of global horizontal irradiance estimates from ERA5 and COSMO-REA6 reanalyses using ground  
653 and satellite-based data, *Sol. Energy*, 164, 339-354, 2018.

654 Van Den Broeke, M. R., Winther, J., Isaksson, E., Pinglot, J. F., Karlöf, L., Eiken, T., and Conrads, L.:  
655 Climate variables along a traverse line in Dronning Maud Land, East Antarctica, *J. Glaciol.*, 45, 295-302,  
656 1999.

657 Van Den Broeke, M. R., Reijmer, C. H., and Van De Wal, R. S.: A study of the surface mass balance in  
658 Dronning Maud Land, Antarctica, using automatic weather stations, *J. Glaciol.*, 50, 565-582, 2004.

659 Van Den Broeke, M., Reijmer, C., and Van De Wal, R.: Surface radiation balance in Antarctica as meas-  
660 ured with automatic weather stations, *Journal of Geophysical Research: Atmospheres*, 109, 2004.

661 Vancoppenolle, M., Timmermann, R., Ackley, S. F., Fichefet, T., Goosse, H., Heil, P., Leonard, K. C.,  
662 Lieser, J., Nicolaus, M., and Papakyriakou, T.: Assessment of radiation forcing data sets for large-scale  
663 sea ice models in the Southern Ocean, *Deep Sea Research Part II: Topical Studies in Oceanography*, 58,  
664 1237-1249, 2011.

665 Vignon, É., Traullé, O., and Berne, A.: On the fine vertical structure of the low troposphere over the  
666 coastal margins of East Antarctica, *Atmos. Chem. Phys.*, 19, 4659-4683, 2019.

667 Wang, C., Graham, R. M., Wang, K., Gerland, S., and Granskog, M. A.: Comparison of ERA5 and ERA-  
668 Interim near-surface air temperature, snowfall and precipitation over Arctic sea ice: effects on sea ice  
669 thermodynamics and evolution, *The Cryosphere*, 13, 1661-1679, 2019b.

670 Wang, G., Hendon, H. H., Arblaster, J. M., Lim, E., Abhik, S., and van Rensch, P.: Compounding tropical  
671 and stratospheric forcing of the record low Antarctic sea-ice in 2016, *Nat. Commun.*, 10, 1-9, 2019a.

672 Wang, Y., Zhou, D., Bunde, A., and Havlin, S.: Testing reanalysis data sets in Antarctica: Trends, per-  
673 sistence properties, and trend significance, *Journal of Geophysical Research: Atmospheres*, 121, 12-839,  
674 2016.

675 Yang, Q., Liu, J., Leppäranta, M., Sun, Q., Li, R., Zhang, L., Jung, T., Lei, R., Zhang, Z., and Li, M.:  
676 Albedo of coastal landfast sea ice in Prydz Bay, Antarctica: Observations and parameterization, *Adv.*  
677 *Atmos. Sci.*, 33, 535-543, 2016a.

678 Yang, Y., Zhijun, L., Leppäranta, M., Cheng, B., Shi, L., and Lei, R.: Modelling the thickness of landfast  
679 sea ice in Prydz Bay, East Antarctica, *Antarct. Sci.*, 28, 59-70, 2016b.

680 Zhang, J.: Increasing Antarctic sea ice under warming atmospheric and oceanic conditions, *J. Climate*,  
681 20, 2515-2529, 2007.

682 Zhang, J.: Modeling the impact of wind intensification on Antarctic sea ice volume, *J. Climate*, 27, 202-  
683 214, 2014.

684 Zhao, J., Cheng, B., Yang, Q., Vihma, T., and Zhang, L.: Observations and modelling of first-year ice  
685 growth and simultaneous second-year ice ablation in the Prydz Bay, East Antarctica, *Ann. Glaciol.*, 58,  
686 59-67, 2017.

687 Zhao, J., Cheng, B., Vihma, T., Yang, Q., Hui, F., Zhao, B., Hao, G., Shen, H., and Zhang, L.: Observa-  
688 tion and thermodynamic modeling of the influence of snow cover on landfast sea ice thickness in Prydz

688 Bay, East Antarctica, Cold Reg. Sci. Technol., 168, 102869, 2019.  
689